Appl. Magn. Reson. 21, 571–585 (2001)

**Applied Magnetic Resonance**



# High-Frequency and -Field Electron Paramagnetic Resonance of High-Spin Manganese(III) in Axially Symmetric Coordination Complexes

**J. Krzystek[1], J. Telser[2], M. J. Knapp[3], D. N. Hendrickson[3], G. Aromí[4], G. Christou[4*], A. Angerhofer[5], and L.-C. Brunel[1]**

[1] Center for Interdisciplinary Magnetic Resonance, National High Magnetic Field Laboratory, Florida State University, Tallahassee, Florida, USA
[2] Chemistry Program, Roosevelt University, Chicago, Illinois, USA
[3] Department of Chemistry, University of California at San Diego, La Jolla, California, USA
[4] Department of Chemistry, Indiana University, Bloomington, Indiana, USA
[5] Department of Chemistry, University of Florida, Gainesville, Florida, USA

**Abstract.** High-frequency and -field electron paramagnetic resonance (HFEPR) has been used to study several complexes of high-spin manganese(III) ($3d^4$, $S = 2$): [Mn($Me_2$dbm)X] and [Mn(OEP)X] (X = $Cl^-$, $Br^-$), where $Me_2dbm^-$ is the anion of 4,4′-dimethyldibenzoylmethane and $OEP^{2-}$ is the dianion of 2,3,7,8,12,13,17,18-octaethylporphine. These non-Kramers (integer spin) systems are not EPR-active with conventional magnetic fields and microwave frequencies. However, use of fields up to 15 T in combination with multiple frequencies in the range of 95–550 GHz allows observation of richly detailed EPR spectra. Analysis of the field- and frequency-dependent HFEPR data allows accurate determination of the following spin Hamiltonian parameters for these complexes: [Mn($Me_2$dbm)Cl], $D = -2.45(3)$ cm$^{-1}$; [Mn($Me_2$dbm)Br], $D = -1.40(2)$ cm$^{-1}$; [Mn(OEP)Cl], $D = -2.40(1)$ cm$^{-1}$; [Mn(OEP)Br], $D = -1.07(1)$ cm$^{-1}$ ($E \approx 0$, and $g \approx 2.0$ in all cases). Comparison of structural data with the electronic parameters for these and related complexes shows quantitatively the effects of axial and equatorial ligation on the electronic structure of Mn(III). These high-spin complexes can be employed as building blocks in the construction of single-molecule magnets. Thus the accurate determination and understanding of the electronic properties, best obtainable by HFEPR, of these monomeric units is important in understanding and improving the properties of the polynuclear single-molecule magnets which can be formed from them.

## 1 Introductoin

Polynuclear transition metal clusters that possess large ground-state spins ($S > 4$) are of significant interest for use as magnetic materials. In particular, high-spin molecules with large-magnitude, negative zero-field splitting (zfs) ($D < 0$) exhibit magnetic hysteresis effects resembling nanomagnets and are termed single-molecule magnets (SMMs) [1–9]. The resultant zfs of a polynuclear complex reflects

* Present address: Department of Chemistry, University of Florida, Gainesville, Florida, USA

the individual ion properties; hence the electronic structure of their monomeric building blocks determines, in part, whether or not a high-spin molecule will also be an SMM.

Among the many paramagnetic transition metal ions, high-spin manganese(III) ($3d^4$, $S = 2$) has been widely employed in efforts to develop SMMs [1–5, 7, 8]. A particular class of complexes that has been successfully used as building blocks for polynuclear Mn clusters with large ground-state spins ($S > 4$) is $[Mn(Me_2dbm)_2X]$ ($X = Cl^-$, $Br^-$), where $Me_2dbm^-$ is the anion of 4,4′-dimethyldibenzoylmethane [2, 3, 10]. An understanding of the electronic properties of the clusters assembled from these monomers requires understanding of those of the constituent units.

Another class of Mn(III) complex that has been used for assembly of magnetic materials employs metal coordination by porphyrinic ligands [11–13]. Again, the electronic structure of the individual complex is crucial in understanding the material's bulk properties. In the present study, we have chosen the porphyrin ligand $OEP^{2-}$ (dianion of 2,3,7,8,12,13,17,18-octaethylporphine) for several reasons. $OEP^{2-}$ complexes are somewhat more soluble than those of, e.g., $TPP^{2-}$ (dianion of 5,10,15,20-tetraphenylporphine); the alkyl substituents in $OEP^{2-}$ provide good shielding for the porphyrin macrocycle π-system, as opposed to the aryl substituents in $TPP^{2-}$, thus providing a slightly more "innocent" ligand; and the $OEP^{2-}$ ligand resembles $Cor^{3-}$ ($Cor^{3-}$ is the trianion of 8,12-diethyl-2,3,7,13,17,18-hexamethylcorrole), which we have also studied by HFEPR [14]. Furthermore, the μ-oxo dimers of $[Mn(OEP)^+]$ have been studied both by magnetic measurements [15] and for their use in catalytic reduction of dioxygen to water [16]. Lastly, the contrast between the $Me_2dbm^-$ and $OEP^{2-}$ complexes allows comparison between square-pyramidal complexes of Mn(III) with an $[O_4X]^{3-}$ ligand donor set versus those having a $[N_4X]^{3-}$ donor set.

One of the most powerful techniques for investigating the electronic structure of the building blocks for magnetic materials (SMMs and extended systems), as well as for the materials themselves, is high-frequency and -field electron paramagnetic resonance (HFEPR) [1, 4, 5, 7–9]. This technique has been successfully applied to mononuclear complexes of high-spin Mn(III) [14, 17–21], a system which is often "EPR-silent" with conventional magnetic fields and microwave frequencies. The present study demonstrates the unique ability of HFEPR to probe the electronic structure of several mononuclear Mn(III) complexes that have relevance to SMMs.

## 2 Experimental

**Synthetic Procedures.** $[Mn(Me_2dbm)_2Cl]$ and $[Mn(Me_2dbm)_2Br]$ were prepared according to published procedures [2, 3]. 2,3,7,8,12,13,17,18-Octaethylporphine ($H_2OEP$) was obtained from Porphyrin Products, Logan, UT, USA. [Mn(OEP)Cl] was prepared by a published procedure [16]. [Mn(OEP)Br] was prepared by an analogous procedure, but with the following modifications: the starting material was $[Mn(OAc)_2 \cdot 4H_2O]$ rather than the chloride salt; complete formation of

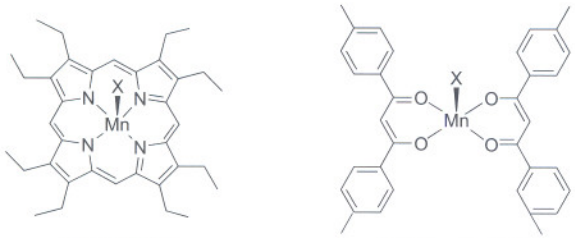


[Mn(OEP)X] [Mn($Me_2$dbm)$_2$X]

**Fig. 1.** Structure of the compounds [Mn(OEP)X] and [Mn($Me_2$dbm)$_2$X], X = Cl, Br.

[Mn(OEP)(OAc)] after refluxing in N,N-dimethylformamide (DMF) for about 1 h was observed by ultraviolet (UV)-visible spectroscopy, at which point an excess of aqueous KBr was added. The product, [Mn(OEP)Br], precipitated immediately. The product was washed with water and methanol, then vacuum dried. Thin layer chromatography with hexanes-$CH_2Cl_2$ (1:1, v/v) indicated a pure product. The structure of [Mn(OEP)X] and [Mn($Me_2$dbm)$_2$X], X = Cl, Br is shown in Fig. 1.

**EPR Procedures.** HFEPR spectra were collected with a spectrometer at the NHMFL that has been previously described [22]. As we have demonstrated previously [14, 20], samples were investigated in each of two forms: as loose powder samples, which often yield field-oriented spectra, and on samples that had been restrained to prevent torquing in the field, which produce powder-pattern EPR spectra. Two complementary methods were used in the latter case: preparing an *n*-eicosane mull, and pressing a KBr pellet. In addition, spectra were collected for [Mn(OEP)X] in low-temperature glasses. The 3:2 mixture of methylene chloride and toluene, carefully purged with dry nitrogen, served as a solvent.

Analysis of powder pattern HFEPR spectra employed a program written by Weihe [23], which is freely available from him [24]. We also used a locally written program to generate field-frequency plots to aid further in the analysis. HFEPR spectra were analyzed with the standard spin Hamiltonian for $S = 2$ composed of electronic Zeeman and zfs (fine structure) terms Eq. (1):

$$\mathscr{H} = \beta B\mathbf{g}S + D\left(S_z^2 - \frac{S(S+1)}{3}\right) + E(S_x^2 - S_y^2). \tag{1}$$

Note that hyperfine terms are omitted, since HFEPR studies on Mn(III) have yet to observe resolved hyperfine splitting from $^{55}$Mn ($I = 5/2$, 100%), for reasons that are not fully understood [25].

## 3 Results

**[Mn($Me_2$dbm)$_2$Cl].** The sample was first measured unrestrained, according to the procedure we developed previously [19]. It was established that the microcrys-

tallites orient in a magnetic field, as do many other Mn(III) complexes with negative zfs [19, 26, 27] (in ref. 27, a single-crystal susceptibility measurement was also performed, and the sign of $D$ was determined to be negative). Although the orientation was incomplete, the parallel $|S, M_S\rangle|2, -2\rangle \rightarrow |2, -1\rangle$ transition is easily recognizable in the spectrum. The resonance field vs. operating frequency dependence of this transition is presented in Fig. 2. The best fit assuming perfectly axial zfs ($E = 0$) yielded the following spin Hamiltonian parameters: $D = -2.35$ cm$^{-1}$, $g_{\|} = 2.04$. These parameters should only be taken as approximations and were subsequently refined by performing an experiment on the sample restrained in a KBr pellet and alternatively in *n*-eicosane mull. A KBr pellet spectrum taken at 280 GHz and 10 K is presented in Fig. 3, accompanied by its simulation with the following spin Hamiltonian parameters: $D = -2.45$ cm$^{-1}$, $E = 0$, $g_{\|} = 2.03$, $g_{\perp} = 2.02$. As proven by the similarity of the experimental and simulated spectra at several frequencies, a random orientation of the microcrystallites with regard to the magnetic field was obtained. The relatively poor signal-to-noise ratio (S/N) for this particular sample resulted in the largest error estimates among all complexes investigated in this study, as shown in Table 1; spectra in *n*-eicosane displayed a very similar S/N ratio. The strong signal at $g = 2.00$ is not present in loose sample; its origin is most probably Mn(II) (e.g., [Mn(Me$_2$dbm)$_2$]), physically induced during the sample grinding and pellet preparation. This is a typical occurrence with Mn(III) complexes. It should be noted however, that the Mn(II) signal is largely isotropic and integration of the spectra, as done previously [14], would show that the total EPR intensity of this species represents only a small part of the total intensity.

**[Mn(Me$_2$dbm)$_2$Br].** The loose sample orients fully in a magnetic field, producing single-crystallike spectra, which at low temperature consist exclusively of the parallel $|2, -2\rangle \rightarrow |2, -1\rangle$ transition (not shown). The plot of the resonance field versus operating frequency of that transition is included in Fig. 2. The best linear fit assuming $E = 0$ yielded the following spin Hamiltonian parameters: $D = -1.46$ cm$^{-1}$, $g_{\|} = 2.01$. The sample was subsequently immobilized in *n*-eicosane, and alternatively in a KBr pellet. An *n*-eicosane spectrum, recorded at 279 GHz and 15 K, is shown in Fig. 4, accompanied by a powder-pattern simulation with the following spin Hamiltonian parameters: $D = -1.40$ cm$^{-1}$, $E = 0$, $g_{\perp} = g_{\|} = 1.98$. Due to an excellent S/N ratio, the error estimates shown in Table 1 are smaller than those for [Mn(Me$_2$dbm)$_2$Cl]. The spectrum shown in Fig. 4 was taken at a higher temperature than that in Fig. 3, so that the excited $|S, M_S\rangle$ states were more populated. Additionally, $|D|$ is smaller for [Mn(Me$_2$dbm)$_2$Br] than for the Cl$^-$ complex, so in combination with the higher temperature, the perpendicular $|2, -1\rangle \rightarrow |2, 0\rangle$ line is the dominant transition. Just to the lower field side of this transition, there is a strong $g = 2.00$ signal, identical to that found in [Mn(Me$_2$dbm)$_2$Cl] and most probably of the same origin (a physically induced Mn(II) complex). Again, its integrated intensity constitutes only a small part of the total EPR intensity, so the Mn(II) signal can be considered a minor impurity.

**[Mn(OEP)Cl].** The loose sample orients in magnetic field, producing spectra that at low temperature consist predominantly of the $|S, M_S\rangle|2, -2\rangle \rightarrow |2, -1\rangle$

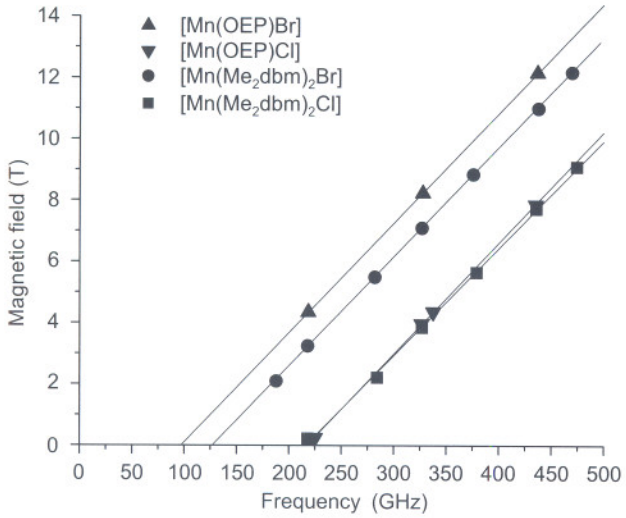


**Fig. 2.** Resonance field vs. frequency dependence of the parallel $|2, -2\rangle \rightarrow |2, -1\rangle$ transition in the solid unrestrained complexes under study. The symbols correspond to experimental resonances, while the straight lines were drawn with the following spin Hamiltonian parameters: $[Mn(Me_2dbm)_2Cl]$: $D = -2.35$ cm$^{-1}$, $g_{\parallel} = 2.04$; $[Mn(Me_2dbm)_2Br]$: $D = -1.46$ cm$^{-1}$, $g_{\parallel} = 2.01$; [Mn(OEP)Cl]: $D = -2.45$ cm$^{-1}$, $g_{\parallel} = 1.98$; [Mn(OEP)Br]: $D = -1.08$ cm$^{-1}$, $g_{\parallel} = 2.00$.

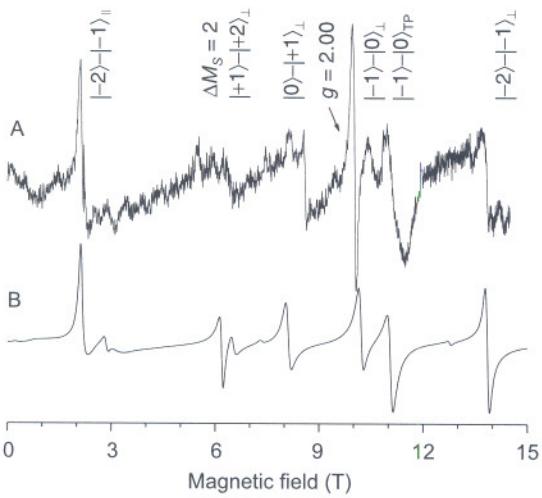


**Fig. 3.** 280.82 GHz spectrum of $[Mn(Me_2dbm)_2Cl]$ in a KBr pellet (A) and its simulation (B). Experimental conditions: temperature, 10 K; field sweep speed, 0.5 T/min from 0 to 12 T and 0.25 T/min from 12 to 14.5 T; modulation frequency, 8 kHz; amplitude, 1.5 mT. Simulation parameters as in Table 1 with single-crystal linewidth of 100 mT for perpendicular, and 50 mT for parallel transitions. Particular transitions showing up in the experiment are identified and labelled accordingly. For clarity, $|S, M_S\rangle$ states are abbreviated as $|M_S\rangle$ states only. "TP" stands for an off-axis turning point. The strong feature appearing at $g = 2.00$ is an impurity, probably Mn(II), and is therefore not reproduced in the simulation.

**Table 1.** Spin Hamiltonian parameters of Mn(III) systems.

| Complex | $D$ ($cm^{-1}$) | $E$ ($cm^{-1}$) | $g_{\parallel}$[j] | $g_{\perp}$[j] |
|---|---|---|---|---|
| Axial complexes | | | | |
| [Mn(OEP)Cl][a] | −2.40(1) | ≤0.02(1) | 2.00(1) | 2.00(1) |
| [Mn(TPP)Cl][b] | −2.290(5) | 0.00(1) | 1.98(2) | 2.005(3) |
| [Mn(Pc)Cl][c] | −2.31(1) | 0.00(1) | 2.00(2) | 2.005(5) |
| [Mn(DPDME)Cl][d] | −2.53(2) | ~0.01 | 2 | 2 |
| [Mn($Me_2$dbm)$_2$Cl][a] | −2.45(3) | 0.00(1) | 2.02(2) | 2.03(2) |
| [Mn(OEP)Br][a] | −1.07(1) | 0.00(1) | 1.98(1) | 2.01(1) |
| [Mn($Me_2$dbm)$_2$Br][a] | −1.40(2) | 0.00(1) | 1.98(2) | 1.98(2) |
| [Mn(DPDME)Br][d] | −1.1(1) | ~0 | 2 | 2 |
| [Mn(OEP)($H_2O$)]($ClO_4$)[e] | −2.3 | — | 2 | 2 |
| Rhombic complexes | | | | |
| [MnCor][f] | −2.64(1) | 0.015(5) | 2.00(1) | 2.02(1) |
| [Mn(tpfc)($OPPh_3$)][g] | −2.69(2) | 0.030(3) | 1.980(4) | 1.994(4) |
| [Mn(dbm)$_3$][h] | −4.35 | 0.26 | 1.97 | 1.99 |
| $Mn^{3+}$ in $TiO_2$[i] | −3.4(1) | 0.116(1) | 1.99(1) | 2.00(2) |

[a] $OEP^{2-}$ is the dianion of 2,3,7,8,12,13,17,18-octaethylporphine; $Me_2dbm^-$ is the anion of 4,4′-dimethyldibenzoylmethane; HFEPR data, this work.
[b] $TPP^{2-}$ is the dianion of 5,10,15,20-tetraphenylporphine; HFEPR data from ref. 20; magnetic susceptibility data for [Mn(TPP)Cl] gave $D = -2.3(2)$ $cm^{-1}$ [31].
[c] $Pc^{2-}$ is the dianion of phthalocyanine; HFEPR data from ref. 20.
[d] $DPDME^{2-}$ is the dianion of deuteroporphyrin IX dimethyl ester; far-infrared data from ref. 34.
[e] Magnetic susceptibility data from ref. 26. These workers formulated the complex simply as [Mn(OEP)×$ClO_4 \cdot H_2O$], however, a subsequent X-ray crystallographic study showed that the water is the axial ligand [15].
[f] $Cor^{3-}$ is the trianion of 8,12-diethyl-2,3,7,13,17,18-hexamethylcorrole; HFEPR data from ref. 14.
[g] $Tpfc^{3-}$ is the trianion of 5,10,15-tris(pentafluorophenyl)corrole; HFEPR data from ref. 21.
[h] dbm is 1,3-diphenyl-1,3-propanedione; HFEPR data from ref. 17.
[i] $Mn^{3+}$ dopant in rutile; EPR data from ref. 32.
[j] The $g$ values were assumed to equal 2 except in EPR studies where they were explicitly determined.

parallel transition (not shown). The plot of the resonance field vs. operating frequency of that transition is shown in Fig. 2. The best linear fit assuming $E = 0$ yielded the following spin Hamiltonian parameters: $D = -2.45$ $cm^{-1}$, $g_{\parallel} = 1.97$. To prevent the field-induced crystallite alignment, we applied the same two methods as described above (*n*-eicosane and KBr pellet). In addition, we dissolved the sample in a 3:2 $CH_2Cl_2$-toluene mixture at a concentration of ca. 100 mM, and froze the solution at low temperature. The low-temperature (10 K) spectra of this solution recorded at 191 and 96 GHz are shown in Fig. 5. Each of the spectra is accompanied by a simulation with a single set of spin Hamiltonian parameters as follows: $D = -2.40$ $cm^{-1}$, $|E| = 0.02$ $cm^{-1}$, $g_{\perp} = g_{\parallel} = 2.00$. Since both operational frequencies shown are smaller than $3|D|$, only perpendicular and partially allowed ($\Delta M_S > 1$) transitions show up in the spectra. The small, rhombic zfs parameter, $E$, introduced in the simulations was necessary to account for the

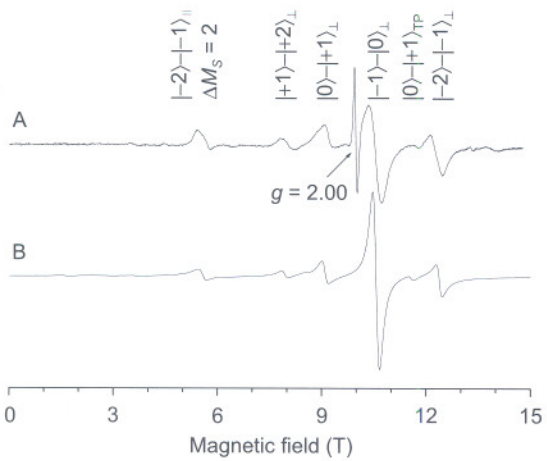


**Fig. 4.** 279.04 GHz spectrum of $[Mn(Me_2dbm)_2Br]$ in eicosane mull (A) and its simulation (B). Experimental conditions as given in legend to Fig. 3 except for temperature equal to 15 K. Simulation parameters as in Table 1 with isotropic single-crystal linewidth of 120 mT. Particular transitions showing up in the experiment are identified and labelled accordingly. The strong feature appearing at $g = 2.00$ is an impurity, probably Mn(II), and is therefore not reproduced in the simulation.

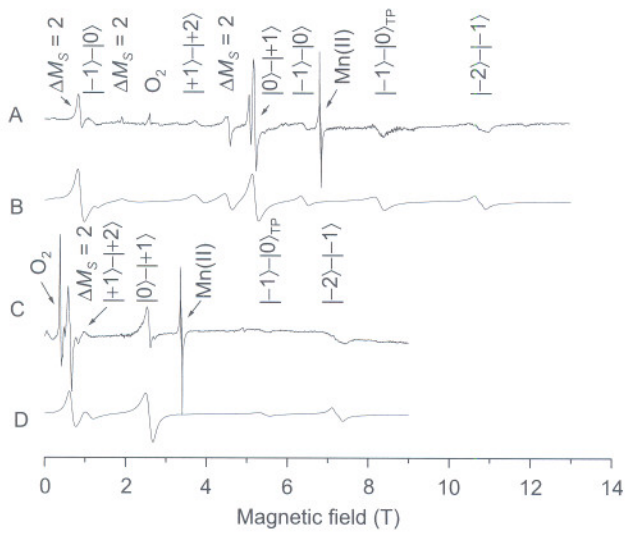


**Fig. 5.** Spectra of [Mn(OEP)Cl] in 3:2 $CH_2Cl_2$-toluene glass at 191.26 GHz (A), its simulation (B), at 95.63 GHz (C) and its simulation (D). Experimental conditions as given in legend to Fig. 3. Simulation parameters as in Table 1 with isotropic single-crystal linewidth of 100 mT. Particular transitions showing up in the experiment are identified and labelled accordingly. All features observed at both frequencies represent perpendicular transitions, except for the features marked "TP", which are off-axis turning points. The strong signals at $g = 2.00$ originate from Mn(II) present as impurity, and the signals at 2.5 T at 191 GHz, and 0.3 T at 96 GHz originate from solid molecular oxygen. Neither is therefore reproduced in the simulations.

increased width of the perpendicular $|2, -2\rangle \rightarrow |2, -1\rangle$ transition at both frequencies. Since that broadening can have other origins, the magnitude of $E$ (0.02 $cm^{-1}$) should be treated as the upper limit for that parameter. The doubling of the $|2, 0\rangle \rightarrow |2, +1\rangle$ transition at 191 GHz could not be reproduced in the simulations with a single set of spin Hamiltonian parameters. This doubling scales with field: it is absent in the same transition at 96 GHz (Fig. 5, spectrum C), but increases at frequencies higher than 191 GHz (not shown). It is thus certainly not caused by a rhombic parameter $E$. Instead, it is likely that there may be two complex sites in the low-temperature glass with slightly different values of the $g$ tensor. This issue will need to be investigated further; however, we note that metalloporphyrins can exhibit structural variability, both in solution and in the solid state [28, 29]. The $g = 2.00$ signal is present in the spectrum, similarly to the previously described complexes. However, its width is smaller than in the solid samples discussed above, and in addition it shows a well-resolved hyperfine sextet characteristic for isotropic Mn(II), which confirms its attribution to the reduced form of manganese. The spectra contain also a weak signal at 2.5 T at 191 GHz and a strong signal at 0.3 T at 96 GHz. Both signals can be attributed to solid molecular oxygen present in the sample despite purging the solvents with nitrogen prior to freezing. This is a rather common feature of all frozen solution HFEPR experiments performed so far [30].

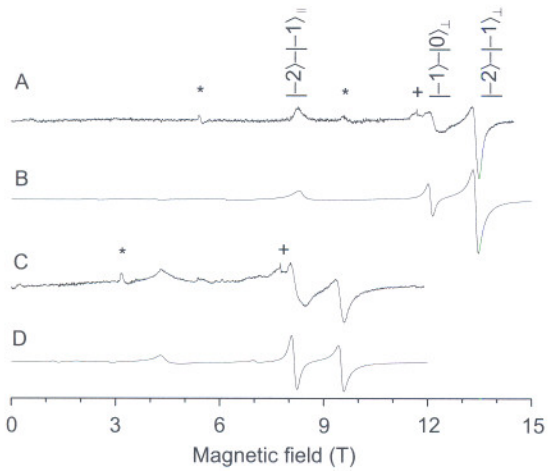


**Fig. 6.** Spectra of loose polycrystalline [Mn(OEP)Br] at 327.85 GHz (A) with its simulation at the same frequency assuming a random distribution of crystallites (B); at 218.55 GHz (C), and powder pattern simulation at the same frequency (D). Experimental conditions as given in legend to Fig. 3 except for temperature equal to 4.2 K. Simulation parameters as in Table 1, with isotropic single-crystal linewidth of 100 mT. Particular transitions showing up in the experiment are identified and labelled accordingly for 328 GHz; the same transitions appear at the lower frequency. The signals around $g = 2.00$ marked with a "plus" originate from an impurity, probably Mn(II), while the signals marked with an asterisk originate from solid molecular oxygen. Neither is therefore reproduced in the simulations. The similarity of experimental and simulated spectra points at an absence of field-induced orientation in [Mn(OEP)Br].

**[Mn(OEP)Br].** Exceptional among the complexes investigated in this study, this particular solid does not undergo field-induced orientation at low temperatures. Therefore, we did not have to immobilize it with methods as above, and performed all experiments on a loose sample. The plot of the resonance field vs. operating frequency of the parallel $|2, -2\rangle \rightarrow |2, -1\rangle$ transition identified in the powder pattern is included in Fig. 2. The best linear fit assuming $E = 0$ yielded the following spin Hamiltonian parameters: $D = -1.08$ cm$^{-1}$, $g_{\|} = 2.00$. The full spectra at 4.2 K and at each of two frequencies, 328 and 219 GHz, are shown in Fig. 6. Each spectrum is accompanied by its powder pattern simulation with a single set of the following spin Hamiltonian parameters: $D = -1.07$ cm$^{-1}$, $E = 0$, $g_{\|} = 1.98$, $g_{\perp} = 2.01$. The experimental spectra also contain weak signals attributed to Mn(II) and molecular oxygen as discussed before. Experiments in a low-temperature 3:2 $CH_2Cl_2$-toluene glass (not shown) yielded very similar results. (We have also studied the complex [Mn(OEP)I], prepared analogously to [Mn(OEP)Br]. Preliminary HFEPR studies suggest a very low magnitude zfs ($|D| \sim 0.1$ cm$^{-1}$). Indeed, in contrast to the other complexes described herein, [Mn(OEP)I] is EPR-visible at X-band microwave frequency in frozen solution. More detailed EPR studies on [Mn(OEP)I], including structural work, are in progress.)

## 4 Discussion

### *4.1 HFEPR Spectroscopy and Analysis*

The procedure employed here to obtain and analyze HFEPR spectra of $S = 2$ systems follows a methodology that we have described in detail previously and that is by now well established [14, 17–21]. The key point is the use of multiple microwave frequencies, formed by harmonic generation from, in this case, two fundamental frequencies ($95 \pm 3$ and $110 \pm 3$ GHz) in combination with swept magnetic fields up to 15 T. The multifrequency capability is extremely useful because of at least three reasons: (a) it allows a rapid evaluation of spin Hamiltonian parameters from field-aligned spectra, (b) it facilitates identifying particular transitions originating from randomly oriented samples, and (c) it increases the accuracy of spin Hamiltonian parameters determined from the spectra. Equally important is the use of computer simulation of both individual powder spectra and of the entire field-frequency-dependent data set for a given complex [14, 20].

The choice of sample form has much bearing on the kind of information extracted from the experiment. The most often used sample form of mononuclear Mn(III) complexes has been polycrystalline solid. It has been shown in this and several previous studies [14, 18–20], that microcrystallites of most Mn(III) complexes orient in field at low temperatures (a phenomenon also called torquing). Torquing is due to a macroscopic alignment of the molecular magnetic moment ($\mu$) within a crystallite. The propensity for torquing is particularly strong in complexes characterized by negative $D$, since such complexes possess an easy axis of magnetization ($\mu_{\|} > \mu_{\perp}$) [27]. Provided that there is sufficient symmetry

within the crystallographic unit-cell, the microcrystallites will align due to this molecular phenomenon, leading to single-crystallike spectra where the magnetic $z$-axis (collinear with $\mu_{||}$) of each molecule is aligned with the external magnetic field.

When torquing does take place, it can be used to the experimentalist's advantage as described both for polynuclear Mn complexes [8] and for mononuclear Mn(III) systems [19], since the spectra obtained resemble those originating from a single crystal. In most cases, however, the field-induced alignment is incomplete, and the resulting spectra are difficult or impossible to interpret. In such a case, dispersing and immobilizing the crystallites prior to introducing the sample into the magnet is desired. This is usually performed with a waxlike substance such as $n$-eicosane (a technique borrowed from magnetic measurements), or pressing the powder with KBr into a pellet (a technique borrowed from infrared spectroscopy). The usefulness of a given method depends very much on the complex of interest.

An alternative way to provide a random distribution of molecules with regard to the magnetic field is to prepare the sample in a low-temperature glass. The choice of proper solvent(s) is of importance in such a case, depending on such factors as the solubility, glass quality, and dielectric losses of millimeter or submillimeter radiation in the given glass, which can be significant at high operating frequencies. Also, a possible interaction of the solvent molecules with the complex of interest must be considered, as we showed in the case of [MnCor] in neat pyridine [14], and for [Mn(TPP)Cl] in a $CH_2Cl_2$-toluene mixture [25].

The result of HFEPR analysis is a set of spin Hamiltonian parameters ($\mathbf{g}$, $D$, $E$) characteristic of the electronic ground state of the complex of interest. Such information can in principle also be obtained by magnetic susceptibility, as was done with several Mn(III) porphyrin complexes [26, 27, 31]. The advantage of HFEPR is that this resonance technique provides higher precision and accuracy in the $g$ tensor and $D$, including the sign of $D$, than do bulk magnetic measurements. In particular, HFEPR spectra of $S = 2$ systems are very sensitive to detection of rhombic zfs ($E \neq 0$), which is quite difficult to detect with powder magnetic susceptibility. Furthermore, HFEPR of high-spin systems in frozen solution, as seen here for [Mn(OEP)Cl], and previously reported for both [MnCor] [14] and [Mn(TPP)Cl] [25] complexes, can provide information on the solution structure of high-spin complexes just as conventional EPR can for $S = 1/2$ systems.

### *4.2 Relation of Structure to Spin Hamiltonian Parameters*

Structural data exist either for the complexes described in this study or for closely related systems. A high-resolution crystal structure of $[Mn(Me_2dbm)_2Cl]$ has been reported [3]. The structure reveals a nearly ideal square-pyramidal complex of Mn(III): the four equatorial Mn-O bonds are almost equivalent (Mn-O length = 0.1892 ± 0.0005 nm) with the Mn(III) ion slightly above the equatorial plane. While the structure of the related $[Mn(Me_2dbm)_2Br]$ has not been deter-

mined, it is expected to be similar due to the relatively minor exchange of an axial $Br^-$ ligand for the $Cl^-$ ligand. Structures have also been reported for [Mn(OEP)Cl] [16], and for [Mn(OEP)($H_2O$)]($ClO_4$) [15]. Both are quite typical of the many structurally characterized porphyrinic complexes of Mn(III) with various axial ligands [28], and both are of very nearly ideal $C_{4v}$ symmetry about the Mn(III) ion. In [Mn(OEP)Cl], the Mn-N bonds are within 0.0004 nm of their average length (0.2019 nm) and the Mn(III) ion is displaced by 0.0280 nm above the plane of the four equatorially coordinated nitrogen atoms [16]. Of particular relevance here, in [Mn(OEP)Cl], the axial Mn-Cl bond length is 0.2385(1) nm [16], while in [Mn($Me_2$dbm)$_2$Cl] the bond length is 0.2380(2) nm [3]. Thus, although [Mn($Me_2$dbm)$_2$Cl] has as an equatorial $[O_4]^{2-}$ donor set and [Mn(OEP)Cl] has a $[N_4]^{2-}$ donor set in a fully π-conjugated macrocyclic ligand, the overall geometry about Mn(III) is very similar in the two types of complexes and the Mn-Cl bond length is almost the same as well. No structure has been reported for [Mn(OEP)Br], but for comparison between axial halide ligands, the Mn-Cl bond length in [Mn(TPP)Cl] is 0.2380(3) nm, which is essentially identical to that for the OEP complex, while in [Mn(TPP)Br], the Mn-Br bond length is 0.2490(1) nm [29]. Similar bond lengths would thus be expected for both [Mn(OEP)Br] and [Mn($Me_2$dbm)$_2$Br].

The structural data show nearly ideal $C_{4v}$ geometry about the Mn(III) ion, whether in porphyrins or in the $Me_2dbm^-$ complexes. This is clearly reflected in the spin Hamiltonian parameters in that the rhombic zfs is negligible, i.e., $E \sim 0$. In contrast, Mn(III) corrole complexes, which do not have fourfold symmetry, exhibit rhombic zfs (see Table 1), although the magnitude of $|E|$ is relatively small [14, 21]. Complexes of Mn(III) for which there is no porphyrinic macrocycle, nor even the bis-bidentate $Me_2dbm^-$ to define an equatorial plane, can exhibit quite substantial rhombic zfs, e.g., [Mn(dbm)$_3$] (see Table 1) [17].

The chief difference among the various complexes described here and elsewhere (see Table 1, especially for data on other porphyrinic complexes of Mn(III)) is the variation in axial ligand. The [Mn(TPP)X] structural data show a smooth increase in Mn-X bond length over the series X = Cl, Br, I [29]. (The structure of [Mn(TPP)I] shows two crystallographically independent molecules, with an average Mn-I bond length of 0.275 nm.) In a simple crystal field approach, this would indicate a weakening of the Mn-X bond over this series, with a strong effect on zfs.

The relation of ligand field to zfs in Mn(III) porphyrins was first pointed out by Dugad et al. [31], who semiquantitatively evaluated the contributions to $D$. We employed their method in our earlier studies of [Mn(TPP)Cl] [20] and [MnCor] [14]. Briefly, for an axially elongated (e.g., square-pyramidal) system, as is the case here for both the $Me_2dbm^-$ and $OEP^{2-}$ complexes of Mn(III), the zfs is expected to be negative ($D < 0$) [31]. As for the magnitude of $|D|$, the equatorial ligand field determines the value of $\Delta$, the $d_{xy}$-$d_{x^2-y^2}$ energy separation, and the axial ligand determines the value of $\delta_1$, the $d_{xy}$-$d_{xz,yz}$ energy separation. These in turn determine the energy splittings between the ground state ($^5B_1$ in $C_{4v}$ symmetry) and the excited $^5B_2$ state ($\Delta = E(^5B_2) - E(^5B_1)$) and $^5E$ state

($\Delta - \delta_1 = E(^5E) - E(^5B_1)$). Spin-orbit coupling with these excited states combines to give $D \approx \lambda^2[-4/\Delta + 1/(\Delta - \delta_1)]$, where $\Delta > \delta_1$ and $\lambda$ is the spin-orbit coupling constant [20, 31]. Thus for a constant equatorial ligand field, such as is the case among a series of porphyrins (or even among different porphyrins, since the organic substituents of the ligand have little effect), variation in the axial ligand field will strongly affect $D$, so that as $\delta_1$ increases (the axial field weakens), the magnitude of $|D|$ will decrease due to diminished coupling with the excited $^5E$ state.

There is, however, another contribution to the zfs, which was pointed out in ref. 32, namely spin-orbit coupling to a triplet excited state ($^3E$) [31]. We defined this contribution as $D' = -4\lambda^2/\delta_3$, where $\delta_3$ is the energy separation between the $^5B_1$ ground state ($d^1_{xy}d^2_{xz,yz}d^1_{z^2}$) and the $^3E$ excited state ($d^1_{xy}d^3_{xz,yz}$). The stronger the overall ligand field, the lower in energy is the triplet excited state and the greater its contribution to the negative value of $D$. This was the case for [MnCor], where the axial field was weak (no axial ligand), but the magnitude of $|D|$ was relatively large, due to this very strong equatorial ligand [14]. The axial ligand field, however, does have an effect on $\delta_3$ so that the overall situation includes competing contributions.

We clarify these several contributions to $D$ by showing their net effect graphically in Fig. 7. In this case, we have used the ligand-field parameters defined by Ballhausen [33], as we did in our previous study [20], which are more fundamentally related to the 3d orbital energy levels. The relation of these parameters, $Dq$, $Ds$, $Dt$, to those used by Dugad et al. [31] is given in the legend to Fig. 7. Within a set of complexes, whether of $Me_2dbm^-$ or of $OEP^{2-}$, the equatorial ligand is constant, so that $Dq$ is constant, and thus the key parameter is $Dt$, which is related to the axial ligand-field strength in that a larger value indicates a weaker tetragonal field ($Dt$ has opposite sign to $Dq$ [33]). All other parameters have been kept constant as well and are based on values and assumptions made in our previous study of [Mn(TPP)Cl] [20].

This discussion can be applied to the compounds of interest here. All of the complexes of Mn(III) with an axial chloro ligand lie within a narrow range: $-2.5 < D < -2.3$ cm$^{-1}$, which is defined by the numerous porphyrinic complexes studied by magnetic measurements, as well as by HFEPR (see Table 1). Although $10Dq$ ($\Delta$) for the $Me_2dbm^-$ complex is likely smaller than that of the porphyrins (here assumed to be 25000 cm$^{-1}$), the $Me_2dbm^-$ complex fits into this range as well. On the basis of Fig. 7, this indicates that all of these Mn(III) complexes with axial chloro ligands have $Dt \approx 2000$ cm$^{-1}$.

The relatively fewer porphyrin complexes with an axial bromo ligand have $D \approx -1.1$ cm$^{-1}$; the $Me_2dbm^-$ complex has a somewhat larger magnitude zfs: $D \approx -1.4$ cm$^{-1}$. Since there are no structural data for this compound, and given the smaller number of bromo-ligated porphyrins in the literature relative to the chloro complexes, we cannot speculate as to the reason for this difference. Nevertheless, all of the Mn(III) complexes with an axial bromo ligand exhibit a magnitude of $|D|$ that is substantially less than that for the chloro-ligated complexes. Use of Fig. 7 suggests that Mn(III) complexes with axial bromo ligands have $Dt \approx 4000$ cm$^{-1}$.

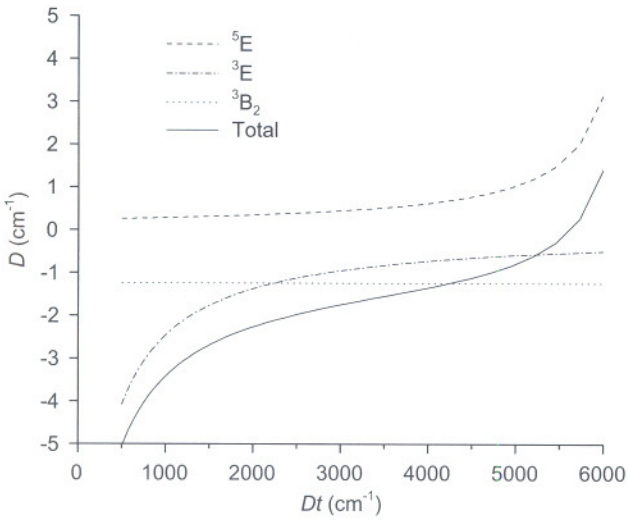


**Fig. 7.** Plot showing the contributions to axial zero-field splitting, $D$, by spin-orbit coupling between the ground state ($^5B_1$) and relevant excited states ($^5B_2$, $^5E$, and $^3E$; all in $C_{4v}$ symmetry). See Krzystek et al. [20] and Dugad et al. [31] for a detailed description of these effects. The independent parameter is the tetragonal ligand-field parameter, $Dt$, as defined by Ballhausen [33]. Other parameters are held constant and appear as follows: $Dq = 2500$ cm$^{-1}$ (where $E(^5B_2) - E(^5B_1) = \Delta = 10Dq$); $Ds = 2500$ cm$^{-1}$ (where $E(^5E) - E(^5B_1) = \Delta - \delta_1$; $\delta_1 = -3Ds + 5Dt$), $B = 1140$ cm$^{-1}$, $C = 3650$ cm$^{-1}$ (where $B$ and $C$ are Racah parameters that determine the free-ion quintet-triplet splitting, so that $E(^3E) - E(^5B_1) = \delta_3 = 6B + 5C - 10Dq + Ds + 10Dt$), $\lambda = 88$ cm$^{-1}$ (where $\lambda$ is the spin-orbit coupling constant for $Mn^{3+}$). The constant contribution to $D$ from spin-orbit coupling of the $^5B_1$ ground state to the $^5B_2$ excited state ($=-4\lambda^2/\Delta$) is shown by a dotted line; the contribution to $D$ from the $^5E$ excited state ($=\lambda^2/(\Delta - \delta_1)$) is shown by a dashed line; the contribution to $D$ from the $^3E$ excited state ($=-4\lambda^2/\delta_3$) is shown by a dot-dashed line, and the sum of these, the total value for $D$, is shown by a solid line.

As mentioned in ref. 31, our EPR results for [Mn(OEP)I] are only preliminary, therefore the situation for iodo ligation can only be discussed qualitatively. [Mn($Me_2$dbm)$_2$I] has not been reported, and although iodo-ligated Mn(III) porphyrins have been prepared successfully [29], both magnetic susceptibility [26] and far-infrared studies [34] on such complexes were unsuccessful. Our EPR data suggest a magnitude of $|D|$ on the order of only 0.1 cm$^{-1}$, clearly less than that for bromo-ligated Mn(III) complexes. Thus the structural trend of increasing bond length over the series Mn-Cl < Mn-Br < Mn-I can be directly related to decreasing magnitude of $|D|$, which can be related to a decrease in axial field, as indicated semiquantitatively for the chloro and bromo complexes by the increase in $Dt$.

## 5 Conclusions

The observation that the axial ligand determines the magnitude of $|D|$ in these monomeric Mn(III) complexes can be used for further design of new SMMs. One goal in this area of chemistry is to discover an SMM which retains its magne-

tization at room temperature. As the magnetic relaxation rate of SMMs is determined by a barrier of size $S^2|D|$, increasing either $S$ or $|D|$ will result in a slower relaxation process. Obtaining a relaxation barrier much greater than thermal energy ($S^2|D| \gg k_BT$) would allow an SMM to act as a magnetic memory device. One approach to make room-temperature SMMs is to synthesize polynuclear clusters composed of single ions with large zfs. It appears that strong axial ligands will increase the magnitude of the single-ion zfs (with $D$ negative) in axially elongated Mn(III) complexes. Therefore, Mn(III)-based SMM design should utilize the strongest axial ligand possible (e.g., from this series Cl preferred over Br over I) in the monomeric building blocks, in order to increase the magnitude of the relaxation barrier.

## Acknowledgements

The following institutions are acknowledged for support: Roosevelt University (JT), NSF (DNH: grants DMR-0103290 and CHE-0095031; GC: grant CHE-0123603). NHMFL is funded by NSF through grant DMR-0084173.

### References

1. Christou G., Gatteschi D., Hendrickson D.N., Sessoli R.: M.R.S. Bull. **25**, 66–71 (2000)
2. Aromi G., Claude J.P., Knapp M.J., Huffman J.C., Hendrickson D.N., Christou G.: J. Am. Chem. Soc. **120**, 2977–2978 (1998)
3. Aromi G., Knapp M.J., Claude J.P., Huffman J.C., Hendrickson D.N., Christou G.: J. Am. Chem. Soc. **121**, 5489–5499 (1999)
4. Artus P., Boskovic C., Yoo J., Streib W.E., Brunel L.-C., Hendrickson D.N., Christou G.: Inorg. Chem. **40**, 4199–4210 (2001)
5. Yoo J., Yamaguchi A., Nakano M., Krzystek J., Streib W.E., Brunel L.-C., Ishimoto H., Christou G., Hendrickson D.N.: Inorg. Chem. **40**, 4604–4616 (2001)
6. Soler M., Artus P., Folting K., Huffman J.C., Hendrickson D.N., Christou G.: Inorg. Chem. **40**, 4902–4912 (2001)
7. Caneschi A., Gatteschi D., Sessoli R., Barra A.L., Brunel L.C., Guillot M.: J. Am. Chem. Soc. **113**, 5873–5874 (1991)
8. Barra A.L., Caneschi A., Gatteschi D., Sessoli R.: J. Am. Chem. Soc. **117**, 8855–8856 (1995)
9. Barra A.L., Caneschi A., Cornia A., Fabrizi de Biani F., Gatteschi D., Sangregorio C., Sessoli R., Sorace L.: J. Am. Chem. Soc. **121**, 5302–5310 (1999)
10. Aubin S.M.J., Dilley N.R., Pardi L.A., Krzystek J., Wemple M.W., Brunel L.-C., Maple M.B., Christou G., Hendrickson D.N.: J. Am. Chem. Soc. **120**, 4991–5004 (1998)
11. Miller J.S., Calabrese J.C., McLean R.S., Epstein A.J.: Adv. Mater. **4**, 498–501 (1992)
12. Miller J.S., Vazquez C., Calabrese J.C., McLean R.S., Epstein A.J.: Adv. Mater. **6**, 217–221 (1994)
13. Miller J.S., Vazquez C., Jones N.L., McLean R.S., Epstein A.J.: J. Mater. Chem. **5**, 707–711 (1995)
14. Krzystek J., Telser J., Hoffman B.M., Brunel L.-C., Licoccia S.: J. Am. Chem. Soc. **123**, 7890–7897 (2001)
15. Cheng B., Cukiernik F., Fries P.H., Marchon J.-C., Scheidt W.R.: Inorg. Chem. **34**, 4627–4639 (1995)
16. Oyaizu K., Haryono A., Yonemaru H., Tsuchida E.: J. Chem. Soc. Faraday Trans. **94**, 3393–3399 (1998)
17. Barra A.-L., Gatteschi D., Sessoli R., Abbati G.L., Cornia A., Fabretti A.C., Uytterhoeven M.G.: Angew. Chem. Int. Ed. Engl. **36**, 2329–2331 (1997)

18. Limburg J., Vrettos J.S., Crabtree R.H., Brudvig G.W., de Paula J.C., Hassan A., Barra A.-L., Duboc-Toia C., Collomb M.-N.: Inorg. Chem. **40**, 1698–1703 (2001)
19. Goldberg D.P., Telser J., Krzystek J., Montalban A.G., Brunel L.-C., Barrett A.G.M., Hoffman B.M.: J. Am. Chem. Soc. **119**, 8722–8723 (1997)
20. Krzystek J., Telser J., Pardi L.A., Goldberg D.P., Hoffman B.M., Brunel L.-C.: Inorg. Chem. **38**, 6121–6129 (1999)
21. Bendix J., Gray H.B., Golubkhov G., Gross Z.: J. Chem. Soc. Chem. Commun. **2000**, 1957–1958.
22. Hassan A.K., Pardi L.A., Krzystek J., Sienkiewicz A., Goy P., Rohrer M., Brunel L.-C.: J. Magn. Reson. **142**, 300–312 (2000)
23. Jacobsen C.J.H., Pedersen E., Villadsen J., Weihe H.: Inorg. Chem. **32**, 1216–1221 (1993)
24. WWW page: http://sophus.kiku.dk/software/epr/epr.html
25. Krzystek J., Pardi L.A., Brunel L.-C., Goldberg D.P., Hoffman B.M., Licoccia S., Telser J.: Spectrochim. Acta (2002) in press.
26. Kennedy B.J., Murray K.S.: Inorg. Chem. **24**, 1557–1560 (1985)
27. Behere D.V., Mitra S.: Inorg. Chem. **19**, 992–995 (1980)
28. Scheidt W.R., Lee Y.J. in: Metal Complexes with Tetrapyrrole Ligands (Buchler J.W., ed.). Berlin: Springer 1987.
29. Turner P., Gunter M.J., Skelton B.W., White A.H.: Aust. J. Chem. **51**, 835–851 (1998)
30. Pardi L.A., Krzystek J., Telser J., Brunel L.-C.: J. Magn. Reson. **146**, 375–378 (2000)
31. Dugad L.B., Behere D.V., Marathe V.R., Mitra S.: Chem. Phys. Lett. **104**, 353–356 (1984)
32. Gerritsen H.J., Sabisky E.S.: Phys. Rev. **132**, 1507–1512 (1963)
33. Ballhausen C.J.: Introduction to Ligand Field Theory, pp. 99–103. New York: McGraw-Hill 1962.
34. Brackett G.C., Richard P.L., Caughey W.S.: J. Chem. Phys. **54**, 4383–4401 (1971)

**Authors' address:** Jurek Krzystek, Center for Interdisciplinary Magnetic Resonance, National High Magnetic Field Laboratory, Florida State University, Tallahassee, FL 32310, USA
E-mail: krzystek@magnet.fsu.edu